October 2004

DESY 04-143
LC-DET-2004-027

# A High-Granularity Scintillator Calorimeter Read Out with Silicon Photomultipliers

V.Andreev [d] V.Balagura [c] B.Bobchenko [c] P.Buzhan [e]
J.Cvach [f] M.Danilov [c] E.Devitsin [d] V.Dodonov [a]
B.Dolgoshein [e] G.Eigen [a,i] L.Filatov [h] E.Garutti *,[a] M.Groll [b]
R.-D.Heuer [b] A.Ilyin [e] M.Janata [f] I.Kacl [f] V.Kantserov [e]
V.Kaplin [e] A.Karakash [e] S.Klemin [h] V.Korbel [a] V.Kozlov [d]
H.Meyer [b] R.Mizuk [c] V.Morgunov [c] E.Novikov [c] S.Němeček [f]
R.Pöschl [a] I.Polák [f] E.Popova [e] A.Raspereza [a] S.Reiche [b]
V.Rusinov [c] F.Sefkow [a] P.Smirnov [d] S.Smirnov [e]
Yu.Soloviev [d] E.Tarkovsky [c] A.Terkulov [d] V.Tikhomirov [d,e]
Š. Valkár [g] J.Weichert [f] J.Zálešák [f]

[a] *DESY, Hamburg, Germany*

[b] *University of Hamburg, Germany*

[c] *Institute of Theoretical and Experimental Physics, Moscow, Russia*

[d] *Lebedev Physics Institute, Moscow, Russia*

[e] *Moscow Engineering and Physics Institute, Moscow, Russia*

[f] *Institute of Physics, Academy of Sciences, Prague, Czech Republic*

[g] *Faculty of Mathematics and Physics, Charles University, Prague, Czech Republic*

[h] *State Unitary Enterprise Science & Production Enterprise (PULSAR), Russia*

[i] *on leave of absence from University of Bergen, Norway*

**Abstract**

We report upon the design, construction and performance of a prototype for a high-granularity tile hadronic calorimeter for a future international linear collider (ILC) detector. Scintillating tiles are read out via wavelength-shifting fibers that guide the scintillation light to a novel photodetector, the Silicon Photomultiplier. A prototype has been tested using a positron test beam at DESY. The results are compared with a reference prototype calorimeter equipped with multichannel vacuum photomultipliers. Detector calibration, noise, linearity and stability are discussed, and the energy response in a 1-6 GeV positron beam is compared with simulations.

The present results demonstrate that Silicon Photomultiplier are well-suited as photodetectors in calorimeters and thus have been selected for the construction of a 1 $m^3$ calorimeter prototype to operate in hadron beams.

*Key words:* linear collider detector, analog calorimeter, semiconductor detectors, scintillator, high granularity
*PACS:* 07.20.Fw, 29.40.Wk, 42.70.Nq, 42.81.Pa, 42.81.Qb

## 1 Introduction

The physics program at the future international linear collider (ILC) [1–3] requires high precision for the reconstruction of heavy bosons (W, Z, H) in hadronic final states. The goal lies in a measurement of jets with an energy resolution of $30\%/\sqrt{E}$ or better [4–6]. Monte Carlo simulations have shown that such a resolution may be achievable, if the concept of "particle flow" [1,7] is utilized in the jet reconstruction. The basic idea here is to combine measured momenta of charged particles with measured electromagnetic energy of photons and measured hadronic energy of neutral hadrons. Thus, high granularity is necessary in both longitudinal and transverse directions for both the electromagnetic and hadronic calorimeters in order to separate photon showers from charged tracks as well as neutral hadron showers from charged tracks and electromagnetic showers.

The CALICE collaboration, has started various R&D projects to design a calorimeter optimized for particle flow. Since high granularity on a large scale may be realized with scintillating tiles read out with wavelength-shifting fibers, a subgroup in CALICE has focused on this technology and has built a small technical prototype consisting of a steel-scintillator sandwich structure (referred to as "MiniCal"). The main motivation was to gain experience in the construction and operation of such detectors for the design of a 1 $m^3$ prototype, which will be used to test the particle-flow concept and to study hadronic shower shapes. Furthermore, the MiniCal is a very suited tool to test system performance of new photodetectors and other detector components.

This publication focuses on the performance of the MiniCal in a positron test beam at DESY. The light yield spread over a hundred tiles is investigated as well as calibration possibilities and reproducibility, and long-term stability monitoring of the system. The light yield optimization of a scintillating tile

* Corresponding author. Address for correspondence: FLC, DESY, Notkestr. 85, 22607 Hamburg, Germany. Tel. +49-40-8998-3779. Fax. +49-40-8998-1812. E-mail: erika.garutti@desy.de

has been the subject of previous R&D studies summarized in Ref. [8]. Since a calorimeter in the ILC detector has to operate in a four Tesla magnetic field, conventional well-established Multianode Photomultipliers (MAPM) are not suitable. Thus, the results presented here were taken with Silicon Photomultipliers (SiPM), a novel photodetector developed by MEPHI-PULSAR in collaboration with DESY [10–12]. For comparison, however, also data with MAPMs were taken. Results for an alternative readout option that is based on Avalanche Photodiodes (APD) will be presented in a separate publication.

## 2 MiniCal structure

In order to perform first R&D studies, establish calibration procedures and test the performance of a high-granularity calorimeter, the MiniCal has been built with the same sampling structure as envisaged for a 1 $m^3$ prototype, consisting of 2 cm thick stainless-steel plates stacked with 0.9 cm gaps. Eleven gaps were equipped with thin-walled aluminum cassettes, each housing nine $5 \times 5$ $cm^2$ wide and 0.5 cm thick scintillating tiles in a $3 \times 3$ matrix as shown in Figure 1a. The MiniCal dimensions have been chosen to minimize fluctuations caused by lateral and longitudinal leakage (in a positron beam of 1-6 GeV) compared to other systematic errors. The 15 cm transverse size of the cassette corresponds to about 6.5 Moliere radii. The material in the MiniCal amounts to 1.15 radiation lengths ($X_0$) and to 0.12 interaction length per layer at normal incidence. The scintillation light of each individual tile is read out separately using a wavelength-shifting (WLS) fiber that is coupled to a photodetector. Further details about MiniCal design, construction and quality control can be found in [9].

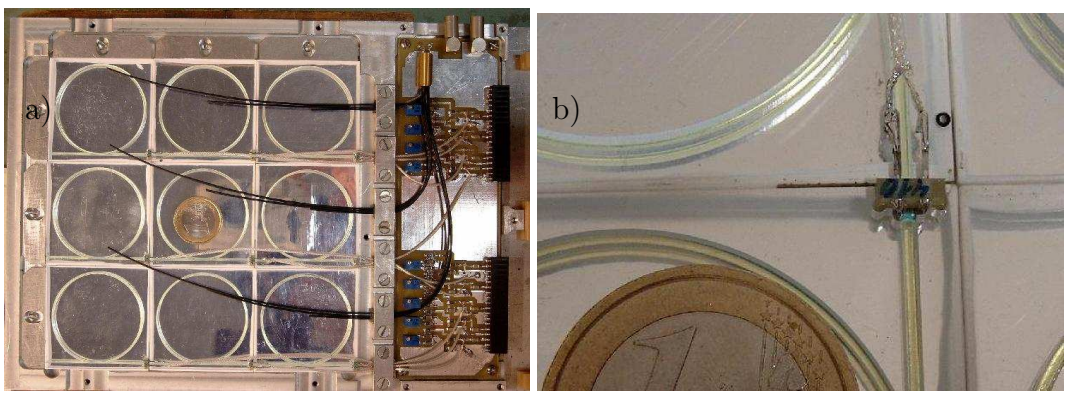


Fig. 1. a) An open cassette housing 9 tiles with a WLS fiber placed in a circular groove read out by a SiPM. b) Zoom on the SiPM connection on tile. The SiPM mounted on a plastic support is inserted in the tile in front of the open end of a WLS fiber. The signal is read out from the two rear pins via a coaxial cable.

The MiniCal is mounted inside an electrically shielded light-tight box that can be positioned horizontally to take beam data or vertically to perform calibrations with cosmic muons. The box is placed on a moving table allowing to aim the beam at a particular transverse position in the cassette.

### *2.1 Scintillator tile-fiber system*

To optimize the light yield of the tile-fiber system various studies of scintillators, tile shapes, fiber configurations and couplings have been carried out during the past two years [8]. Thus, the group obtained tremendous expertise for the assembly of a large number of tiles with very high efficiency and low light yield spread.
For SiPM readout a plastic scintillator (BASF 130) produced by the Vladimir company (Russia) has been chosen. The tile edges are chemically treated to produce small reflecting bubbles on the surface. This technique producing efficient diffuse reflectors is thus suited for large quantity applications. A 1 mm thick green WLS fiber is inserted in a circular groove on the tile. The WLS fiber is a double clad type (Y11, 300 ppm) from Kuraray. The total length needed for one tile is about 13 cm. The fiber ends are cut with a special zirconium-dioxide blade that provides surface quality comparable to polishing. One end of the WLS fiber is connected via a $\sim$100 $\mu$m air gap to the SiPM mounted on the tile. The open end of the WLS fiber, and the tiles upper and lower surfaces are covered with reflector foil (VN2000, superradiant produced by the 3M company). The light yield with such optimized tile-fiber systems is $\sim$200 photons per minimum ionizing particle (MIP), which is sufficient for SiPM readout. The light yield non-uniformity over a tile, excluding the tile edges, is about 4%. At the tile edges the light yield loss is at most 20%. The optical cross talk through the chemically treated edges of neighboring tiles is smaller than 2.5% [9].
The tile-fiber system for readout with multianode vacuum phototubes is slightly different. In this case BICRON BC408 scintillator material is used, which yields a factor 1.5 more light than the BASF 130 scintillator. The same type of WLS fiber is housed in a 7.5 cm quarter-circle groove. An additional $\sim$ 50 cm of WLS fiber are needed to connect the vacuum phototube which is mounted on a window on the MiniCal light tight box. The tiles are entirely wrapped with reflector foil since the edges in this case are not chemically treated. This system also produces a light yield of $\sim$200 photons per MIP.
The construction procedure has been tested on a sample of over 130 pieces for the latter configuration and a light yield spread of 7% is achieved. For each tile the homogeneity is better than 4% for more than 90% of the area.

*2.2 Silicon photomultiplier*

The SiPM is basically a pixelated avalanche photodiode operated in the limited Geiger mode [10–12], thus achieving gains of the order of $\sim 10^6$ per pixel, similarly as those in vacuum photomultipliers. In present devices, the detector surface of 1×1 mm$^2$ is divided into 1024 pixels. The detectors are operated with a reverse bias voltage that is 10-15% above the so-called breakdown voltage, *i.e.* the point at which the current starts to increase very rapidly with a slight increase of the reverse bias voltage. In each pixel the current flow is limited by an individual polysilicon resistor ($R_{pixel} = 400k\Omega$). Provided that all pixels operate as independent detectors, the signal from one pixel is determined by the charge accumulated in the pixel capacitance, $C_{pixel}$, *i.e.* $Q_{pixel} = C_{pixel}\Delta V = C_{pixel}(V_{bias} - V_{breakdown})$, where the voltage difference $\Delta V$ is of the order of a few volts, $C_{pixel}$ is typically 50 fF, yielding $Q_{pixel}$ of the order of 150 fC or $10^6$ electrons.
The SiPM pixel signal does not depend on the number of primary carriers (because of the Geiger mode). Thus, each pixel detects the carriers created by a photon, ionization of a charged particle, or thermal noise with the same response signal of $\sim 10^6$ electrons. For such a gain cross talk between adjacent pixels is observed at a level of $20 - 30\%$ at room temperature. Analog information is obtained in this device by adding the response of all pixels fired

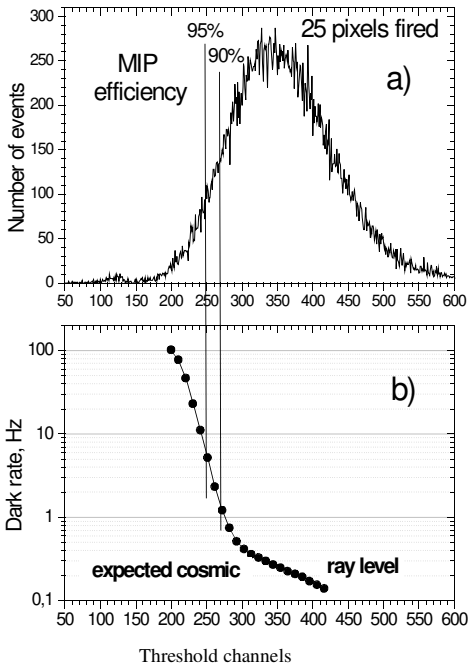


Fig. 2. a) Pulse height spectrum of $\beta$-electrons from a Sr$^{90}$ source for a MiniCal tile. The pedestal peak is in channel 120. b) SiPM dark rate as a function of threshold.

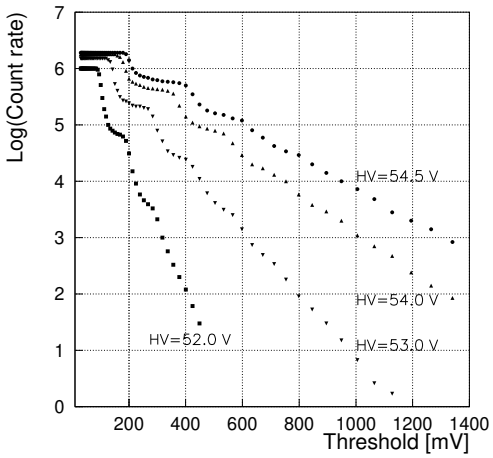


Fig. 3. Dark rate dependence on threshold for different bias voltages of a 1024-pixels/mm$^2$ SiPM at room temperature.

as digital counters. The dynamic range is determined by the finite number of pixels, presently $\sim 10^3$.
The SiPM photon-detection efficiency is comparable to the quantum efficiency of photomultipliers for blue light and somewhat larger for green light, which is important for the usage of WLS fibers. The photon detection efficiency, inter-pixel cross talk and gain increase with $\Delta V$ [12].
For stable operations the sensitivity of the SiPM gain and efficiency to temperature and bias voltage is an important issue. The total temperature and bias voltage dependence of the SiPM gain at room temperature is measured to be 4.5%/°C and 7%/0.1V.
Due to their compactness SiPMs can be embedded in the scintillator tile as shown in Figure 1b. The pulse height spectrum of $\beta$-electrons from a Sr$^{90}$

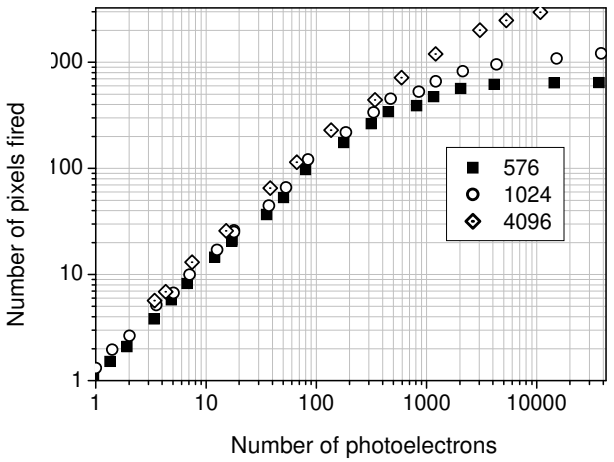


Fig. 4. Nonlinear response to a 40 ps laser light-signal for SiPMs with different number of pixels.

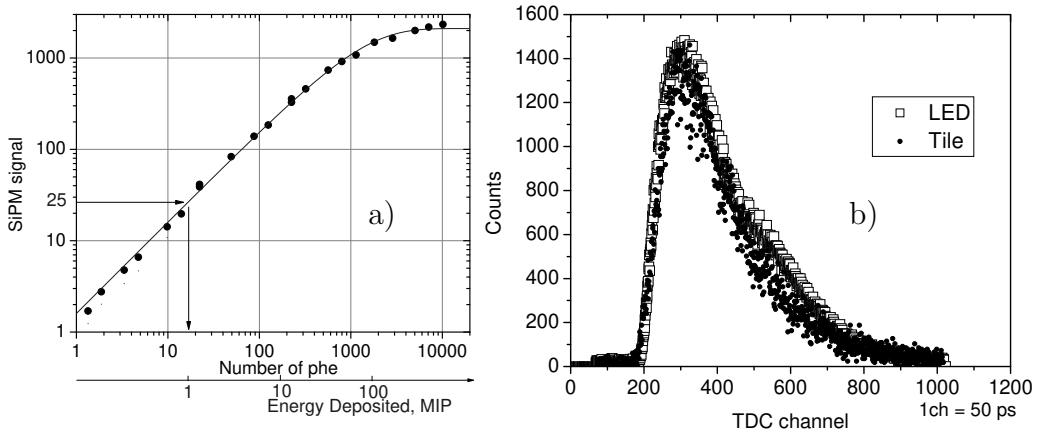


Fig. 5. a) Nonlinear response to an LED light signal for 1024-pixels/mm$^2$ SiPM. b) Time shape of the used LED light signal (open squares) compared to the tile-fiber system signal (points). On the x-axis 1 ch. = 50 ps.

source recorded with this tile-fiber system is shown in Figure 2a.
There are some limitations of the usage of such a readout system for tile calorimeters: the first limiting factor is the dark rate at a threshold, which ensures 90-95% of MIP detection needed for the reconstruction of MIP tracks inside hadronic showers. MIP detection is also important because the HCAL is assumed to be calibrated in self-triggering mode using cosmic muons. Therefore, the SiPM dark rate has to be of the order of the cosmic muon rate or smaller (see Figure 2b). At high threshold (high number of pixels) the SiPM dark rate is determined by the inter-pixel cross talk which is strongly dependent on the bias voltage. The threshold dependence of the dark rate is shown in Figure 3 for various bias voltages. The requirement to have a sufficiently low dark rate limits the SiPM gain to the level of $10^6$ and its photon detection efficiency to 10-12% [12] at room temperature in the case of tile HCAL application. Another limitation is given by the finite number of pixels introducing a nonlinearity of the SiPM signal, when the number of produced photoelectrons

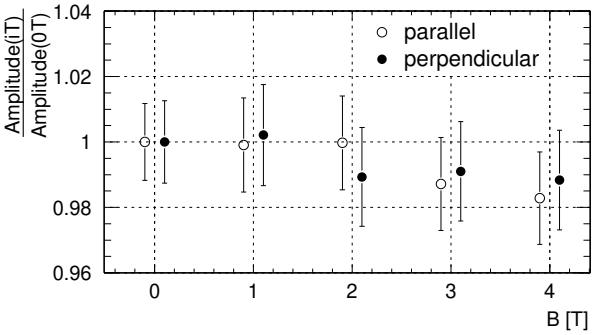


Fig. 6. SiPM signal amplitude dependence on magnetic field for the two orientations of the field perpendicular and parallel to the photodetector surface.

is of the order of the total number of pixels. Figure 4 presents the linearity range of the SiPM for a short laser light pulse of 40 ps, showing saturation effects for large signals.
Due to the fast pixel recovery time, the SiPM response depends on the width of the light pulse. The duration of the light signal produced in the MiniCal tile-fiber system is typically ∼10 ns FWHM (see Figure 5b). In this case the SiPM saturation occurs at about 2000 pixels for a SiPMs with 1024 pixels/mm$^2$ as shown in Figure 5a. This indicates that the effective recovery time for a pixel is rather small (∼10 ns) and each pixel is fired approximately twice on average when recording a signal from the tile-fiber system.
Since the SiPM have to function properly in a magnetic field, their operation has been tested at DESY in magnetic fields up to 4T for two orientations of the field: parallel and perpendicular to the detector surface. The light amplitude of a LED signal has been recorded as a function of the magnetic field in comparison to zero-field measurement. As shown in Figure 6 the SiPM signal is constant within the 1% measurement accuracy. Furthermore, the dark current, noise frequency, gain and pixel cross talk of a SiPM have been measured at 4T and found to be magnetic field independent [13].

### *2.3 Multi-channel photomultiplier*

Reference measurements are presented, which are performed with the MiniCal using 16-pixel multianode photomultipliers (MAPM) from Hamamatsu (H6568). These devices have an anode pixel size of 4 x 4 mm$^2$, and a gain on the order of $10^5$, when operated at a high voltage of 700-800 V [1] . Thus, a preamplifier of gain 10 is also needed, which introduces additional noise to the output signal. The gain variation between the 16 pixels operated with common high voltage can be as large as 40%. The gain is temperature independent to better than 1%/°C. The typical quantum efficiency of the MAPM is about 11% in the wavelength range of the green WLS fiber.
Due to the large pixel size, up to four WLS fibers can be connected to each channel allowing to read out independent tiles or groups of tiles combined in the beam direction. In the latter configuration the light yield spread between the tiles cannot be compensated by individual calibration. This leads to an increase in resolution.
For the studies presented here, the central tile of each layer in the MiniCal were read out individually, while due to the limited number of readout channels the surrounding tiles of three subsequent layers were read out by one MAPM channel.

[1] The operation at relatively low values of high voltage minimizes the channel-to-channel gain fluctuations.

## 3 Test beam setup

The MiniCal tests were conducted in the DESY test beam 21 facility. The positrons are produced from the DESY II electron synchrotron. The primary electrons in the synchrotron hit a thin wire and radiate Bremsstrahlung photons that are extracted and converted into $e^+e^-$ pairs in a 1 mm thick Cu target. A deflecting magnet separates $e^+$ and $e^-$. By varying the field of the magnet beam energies of 1-6 GeV can be selected by a collimator. The beam energy spread from the smallest collimator slit ranges from 6% at 1 GeV to 2% at 3-6 GeV. The beam intensity reaches $10^3$ $e^+$ cm$-2$ s$-1$ . The beam has a bunch rate of 1 MHz and a bunch length of around 30 ps.
A beam trigger is obtained by requiring coincident hits from two perpendicular scintillator counters with a cross section of $2 \times 2$ mm$^2$ and a veto signal from a hole counter. In addition, a pedestal/noise and an LED trigger are installed. The analogue signal from the SiPMs is directly sent to a LeCroy 2249A 10-bit charge sensitive ADC via 25 m long shielded coaxial cables. The typical MIP pulse size is 2.5 pC in 20 ns, with a fall time of $\sim$60 ns. For gain calibration, the signal is amplified by a factor of 20. A trigger gate of 100 ns is used for the ADC. The ADCs are read out via CAMAC with a speed of about 700 events/sec for 240 ADC readout channels.
The data are first stored in binary format on a Linux PC, then converted into standard Linear Collider Input/Output format (LCIO) [14] or ROOT files for the analysis.

## 4 MiniCal calibration

The calibration in the MiniCal prototype is performed using the peak position of minimum ionizing particles (MIP) with respect to the pedestal, since this separation is easily determined from the data. Since each individual channel is calibrated, different light yields in the tile as well as different photodetector responses, preamplifier gains and ADC conversions are accounted for. The calibration has been performed using MIPs from cosmic muons and from the $e^+$ beam. For the latter calibration all cassettes are removed from the absorber plates and are stacked next to them. The beam is steered at the center of a tile in the $3 \times 3$ matrix. To reduce second-particle effects a MIP signal is required in the last layer. In this approach all eleven longitudinal layers can be calibrated at the same time. With nine beam settings all tiles are calibrated. The two methods give compatible results within the calibration accuracy of about 1%. Since the beam calibration is rather fast, it has been adopted for daily checks of reproducibility.
The typical pulse height distributions for a MIP signal from MAPM and SiPM are compared in Figure 7. To fit the MIP spectrum a Gaussian function is used

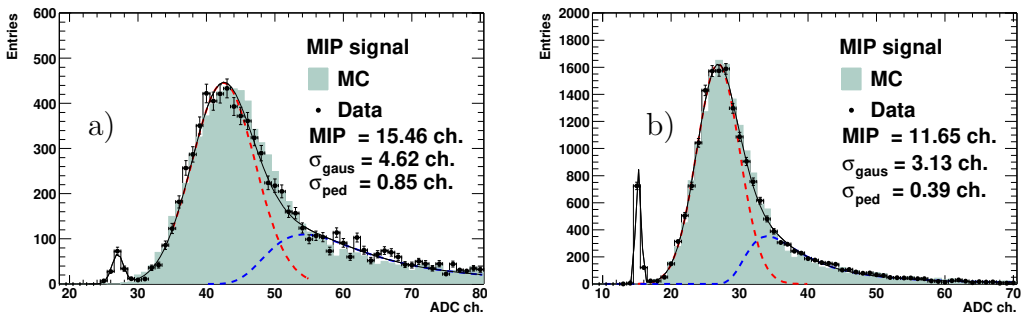


Fig. 7. MIP spectrum from MAPM (a) and SiPM (b), fit with the function described in section 4 (solid line). The dashed lines show the contribution of the Gaussian and Landau functions to the fit. The MC prediction (full histogram) is discussed in section 5.

to describe the pedestal, and a linear combination of a Gaussian function and a Landau function[2] to describe the MIP distribution. The resulting fit is shown by the solid line, while the dashed lines indicate the individual contributions of the Gaussian and Landau functions to the fit. For each tile, the MIP amplitude is approximated by the separation of the two Gaussian peaks, MIP = S = $A_{gaus} - A_{ped}$, yielding a calibration of the corresponding ADC channel in MIPs.

To compare the noise of the two readout systems, the ratio of the MIP amplitude to the Gaussian width of the pedestal distribution N = $\sigma_{ped}$ is used as a figure of merit. The average S/N ratio is ∼17 for MAPM and ∼30 for SiPM. The MAPM ratio is worse due to the additional preamplifier in the signal readout chain.

The ratio S/$\sigma_{gaus}$, with $\sigma_{gaus}$ representing the Gaussian width of the MIP signal, expresses the separability between signal and pedestal, which is a useful quantity for setting a limit for a possible threshold cut. For MAPM and for SiPM the measurements yield S/$\sigma_{gaus}$ ∼3.3±0.1 and ∼3.7±0.1, respectively, indicating that the photoelectron statistics are similar in both systems as expected.

### *4.1 Calibration reproducibility and homogeneity*

A crucial point of this study is to monitor the reproducibility of the calibration of more than 100 tiles. Since the calibration is performed with a beam of much smaller size compared to the tile size, the homogeneity of the tile surface has been investigated in order to assign a systematic uncertainty to this calibration procedure. For this purpose an eight-point scan was performed in steps of

[2] The Landau function is taken from: K.S. Kölbig and B. Schorr, A program package for the Landau distribution, Computer Phys. Comm. 31 (1984) 97-111.

1 cm around the center of a tile with quarter-circle fiber. The MIP calibration factors have been evaluated for each position and a maximum variation of 2% in amplitude is observed for the entire set of calibrated tiles. Therefore, a maximum systematic uncertainty of 2% is quoted for the calibration procedure to account for the inhomogeneity of the single tile response.
Calibration factors were measured daily over a period of one month for the central 12 tiles of the MiniCal prototype with MAPM readout. A fluctuation of 1.6% is observed in the extracted values, which is inside the systematic accuracy of this measurement.

### *4.2 LED monitoring of the response*

An LED system has been installed to monitor the stability of the readout chain versus time. Clear fibers of 0.8 mm in diameter distribute blue LED light either directly to the MAPM channels or illuminate the scintillating tile close to the SiPM. The same LED light is also sent to a PIN diode for monitoring the LED light emission. The PIN diode response is used to correct possible intensity variations of the LED light. The LED is pulsed at a frequency of 1 Hz. The stability of the monitoring system has been checked after PIN diode correction and found to be better than 1.5% over periods of several days. Since for present measurements data taking periods were rather short (10-40 min), voltage and temperature variations were sufficiently small that corrections were not necessary. Studies, however, have shown that this monitoring system produces corrections resulting from an average over a data taking period with an accuracy of $\sim$1%.

### *4.3 SiPM calibration*

For SiPM operation, in addition to the MIP calibration a pixels/MIP calibration is required to convert the response function presented in section 2.2, which is expressed as the number of fired pixels versus the number of photoelectrons (pe). By amplifying the SiPM signal by a factor of 20, it is possible to observe the single photoelectron peak spectrum from a low intensity LED light. The MIP signal is also measured with the same electronic setup. An example of SiPM pulse height spectrum (at room temperature) used for this calibration is shown in Figure 8a. In Figure 8b calibration factors obtained with a $Sr^{90}$ $\beta$-source are compared to factors obtained from beam calibration. A very good correlation is shown for the two sets of measurements. The average calibration factor obtained for all 99 channels is 25$\pm$4 pixels/MIP. By applying this average factor the SiPM response function is recalibrated and

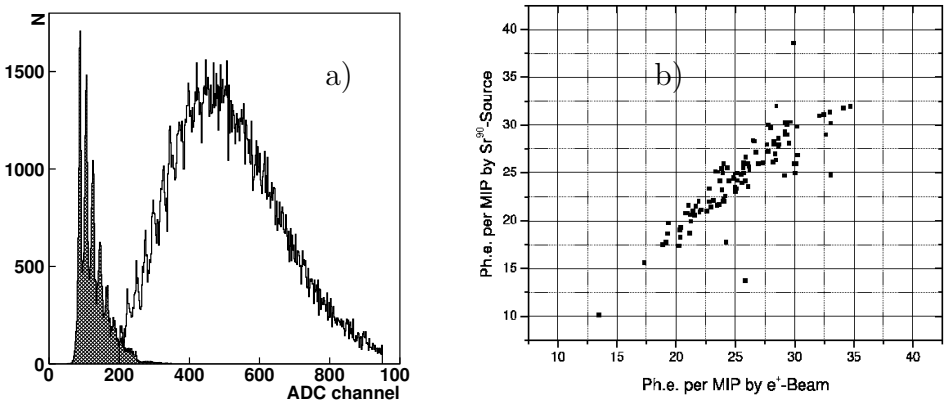


Fig. 8. a) SiPM pulse height spectrum for low intensity LED light (shaded area) and for a MIP signal from $\beta$-source. b) Correlation of calibration factors obtained with a $\beta$-source and a 3 GeV $e^+$ beam for all 99 tiles in the MiniCal readout by SiPMs.

used to correct the SiPM measurement. The value of the energy sum for each beam energy obtained with this procedure agrees within less then 0.5% with the same value obtained calibrating each tile individually.

## 5 Simulation of the detector response

The electron shower evolution has been simulated by implementing the MiniCal geometry into the GEANT4 [15] framework. For an ideal detector response an energy resolution of $18.5\%/\sqrt{E[GeV]} \oplus 2\%$ [3] is expected from the energy deposition in 11 layers. The constant term of 2% is mainly due to shower leakage. Up to 4% of the total energy for a 6 GeV beam escapes the MiniCal, while lateral leakage is negligible.
To obtain a more detailed description of the real detector performance, physical effects need to be implemented in the MC such as photodetector efficiencies, photodetector noise, beam energy resolution, calibration uncertainties, etc. The flowchart of the implementation is drawn in Figure 9. In each tile, the real energy deposited is defined as $E_{real}$. The scintillator and WLS-fiber convert $E_{real}$ into photons, which are then converted into photoelectrons ($N_{pe}$) for MAPM data or into fired pixels ($N_{pixel}$) for SiPM data with fluctuations represented by Poisson statistics. The total charge is recorded with a charge-sensitive ADC calibrated in MIPs ($N_{ADC}$). The conversion factors for ADC channels per MIP are determined in two steps: first, we determine $N_{pixel}$/MIP from the single photoelectron peak for the SiPM readout and $N_{pe}$/MIP from

[3] The symbol $\oplus$ indicates the sum in quadrature of the two terms.

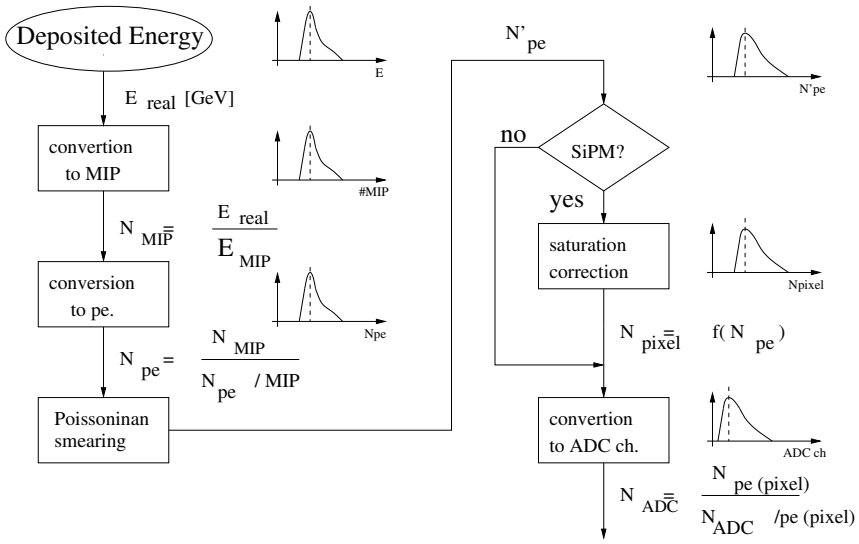


Fig. 9. Flowchart of Monte Carlo implementation of photodetector physics.

the signal width for MAPM; second, we calibrate $N_{ADC}$/pe adjusting the position of the MIP peak. In case the simulated detector is the SiPM, the response function presented in section 2.2 is used to describe the non-linear relation between number of photoelectrons and number of fired pixels. In Figure 7, pulse height spectra in units of MIPs are shown compared to the MC prediction for both MAPM (a) and SiPM (b) after including the photodetector properties. In both cases the MIP spectra are well reproduced by the simulation.
The beam energy spread described in section 3 has been included in the MC description.

## 6 Shower profile description

A good reconstruction of the shower shape will be a crucial requirement in the operation of the final detector. In the case of electromagnetic showers MC simulations should offer an almost perfect prediction, allowing to verify the modeling of detector effects. Once a reliable and detailed detector understanding is achieved, the major task of the MC is to simulate hadronic showers. This is a much more complex task, which will be the aim of the studies with a larger prototype to be built next.
The longitudinal development of the electromagnetic shower in the 11 layers of the MiniCal is shown in Figure 10. The energy deposited is expressed in number of MIPs. Spectra taken from the calibrated SiPM response for 3 GeV beam are compared to MC prediction for each layer. The lateral shower shape is presented in Figure 11 for the fourth layer of the MiniCal structure. The $e^+$ shower is essentially contained in the central tiles. The MC gives in both cases a reasonable description of the shower profiles.

## 7 Linearity and energy resolution

Figure 12a shows the energy deposition summed over all tiles of the 11 layers of the MiniCal prototype obtained with SiPM (circles) and MAPM (squares) readout for beam energies ranging from 1 GeV to 6 GeV. A linear fit is performed to the data to extract the slope parameter in units of MIP/GeV. The slopes for the two photodetectors agree at the 2% level. By constraining the fit to the zero point the slope changes by 2% with respect to the unconstrained fit. The linear behavior of the SiPM result (better than 2%, as seen in Fig-

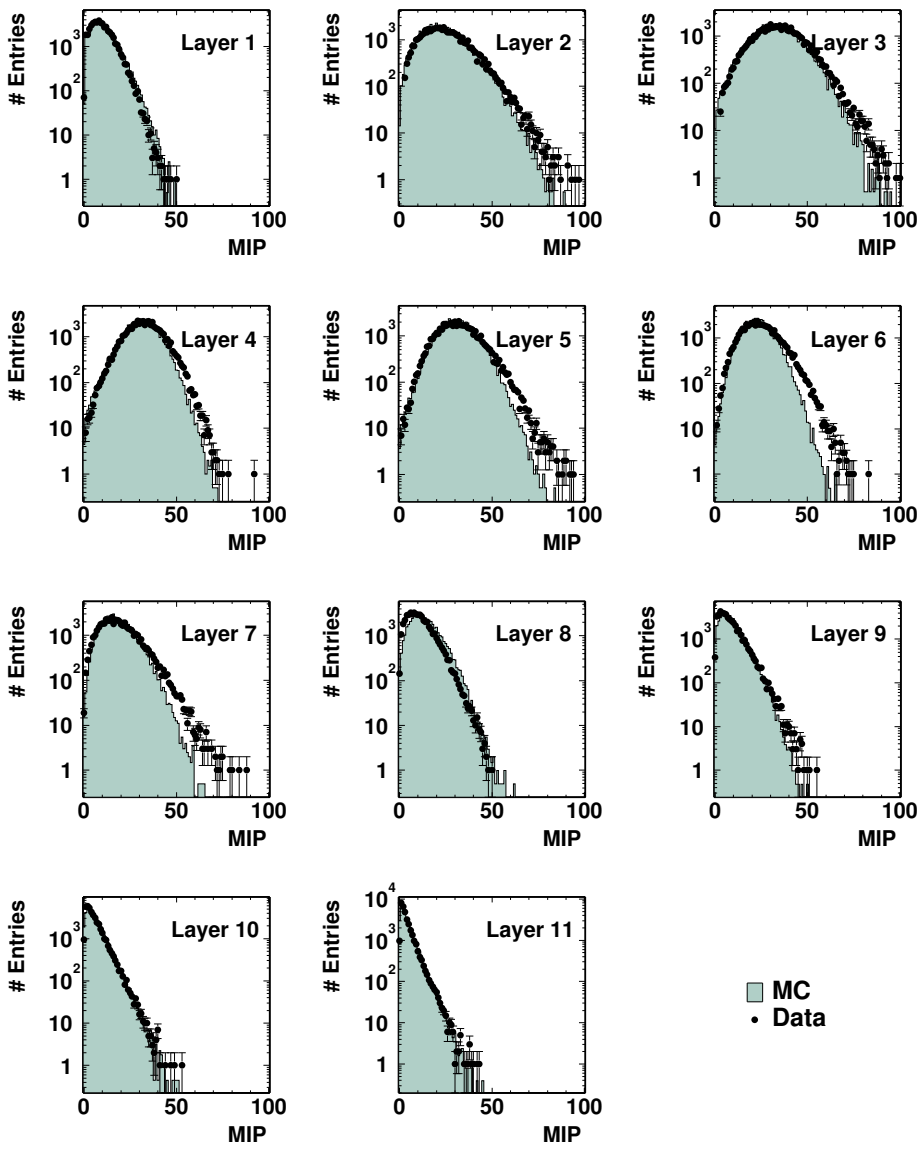


Fig. 10. Data (points) to MC (shaded histogram) comparison of the electromagnetic longitudinal shower for a 3 GeV incident $e^+$ beam. The spectra expressed in number of MIPs refer to individual tiles with SiPM readout.

ure 12b) demonstrates that the applied saturation correction is reliable. The magnitude of such a correction can be as large as 15% at 6 GeV as the uncorrected data (open circles) indicate. The MC prediction for the total number of MIPs including detector response and beam energy spread is also in good agreement with the data as shown in Figure 12a (triangles).

The energy resolution for the two data sets is plotted in Figure 13. The stochastic terms of the energy resolution for both SiPM data and MAPM data, extracted from maximum likelihood fits, are in very good agreement. In both cases, a value of the order of 21% is obtained that is also well reproduced by the MC simulation. The constant term is about 2% as expected from the MC simulation. The very good agreement between SiPM and MAPM results shown in Figure 13 implies that the non-linearity of SiPM does not affect the

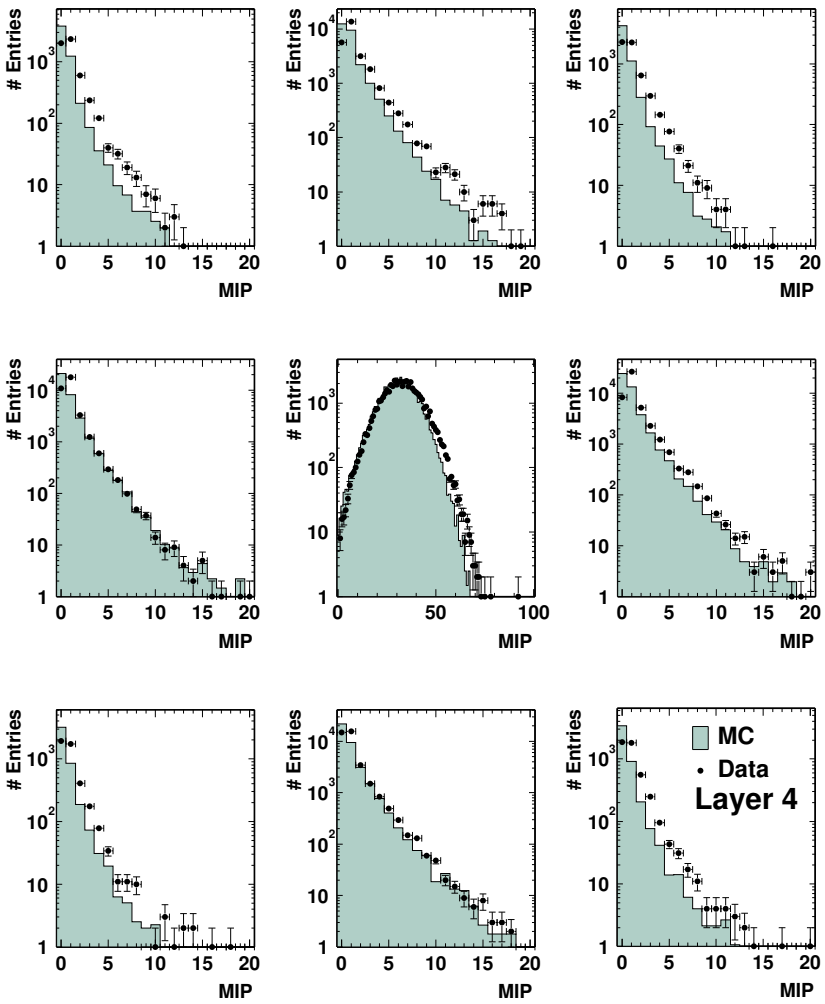


Fig. 11. Data (points) to MC (shaded histogram) of the electromagnetic transverse shower for a 3 GeV incident $e^+$ beam. The spectra expressed in number of MIPs refer to individual tiles with SiPM readout.

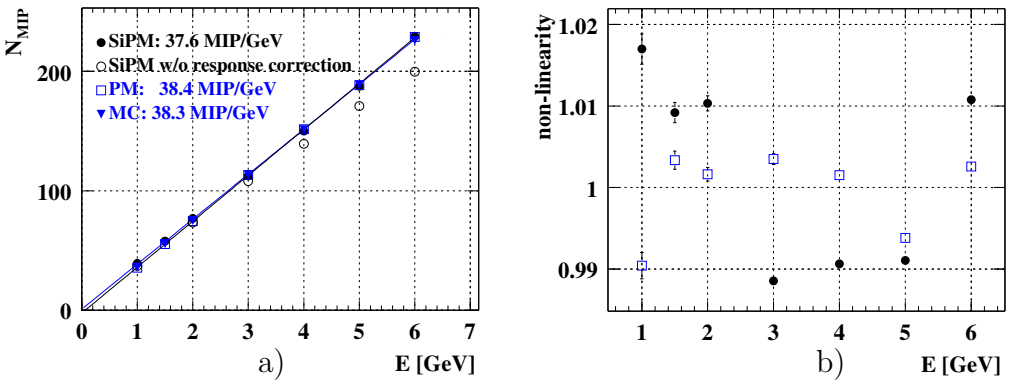


Fig. 12. a) Total signal normalized to number of MIPs versus beam energy, where solid points (open circles) show SiPM data with (without) response function correction, squares MAPM data and triangles MC prediction respectively. b) deviation of the measurements from a linear fit.

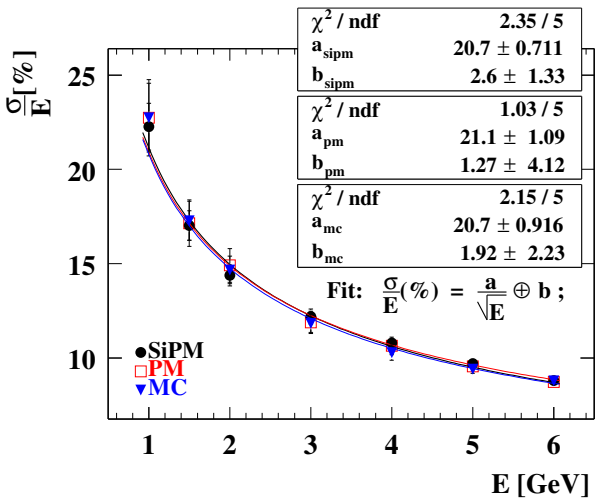


Fig. 13. Measured energy resolution for SiPM with (solid points), MAPM (squares) and MC prediction (triangles).

energy resolution in the range probed here.
The error includes both statistic and systematic uncertainties added in quadrature. The statistical error is typically of the order of 1.6-1.8%. The main source of the systematic uncertainties is electronic noise (pedestal), which contributes more significantly at low energies than at high energies (spanning from 5% to 2% for SiPM and from 8.4 to 3.3% for MAPM). The uncertainty due to photodetector non-linearity is 1.5% for SiPM and less than 1% for MAPM.

## 8 Conclusion

A calorimeter concept for a linear collider detector has been developed, which allows unprecedented longitudinal and transverse granularity. The SiPM has been established as an excellent photodetector for recording the green light of a wavelength shifting fiber that collects the light of individual scintillating tiles. As an important step towards mass production, a first calorimeter prototype equipped with 99 SiPM, has been successfully designed, constructed and operated in an $e^+$ test beam. A reliable calibration procedure for all calorimeter cells has been established. A monitoring system has demonstrated a rather stable detector operations. Using a single function for all photodetectors the non-linear response of the SiPM has been corrected to better than 2%. A detailed MC simulation has been developed to interpret the test beam data, which correctly models the SiPM response. The MiniCal operation has provided valuable experience for the design, construction and operation of a 1 $m^3$ prototype, that is presently under development and will be completed in 2005. This prototype will be tested together with an electromagnetic calorimeter prototype in hadron beams to study hadronic shower shapes, perform shower separations and test the concept of particle flow.

## 9 Acknowledgments

We would like to thank the technicians and the engineers who contributed in the design and construction of the prototype. We also gratefully acknowledge the DESY management for its support and hospitality, and the accelerator staff for the reliable and efficient beam operation. This work is supported by the contribution of Bundesministerium für Bildung und Forschung, Germany; Alexander von Humboldt Foundation(Researce Award IV,RUS 1066839 GSA),INTAS(Grant # YSF150-00); the Russian grants SS551722.2003.2 and RFBR0402/17307a; the Ministry of Education of the Czech Republic under the project LN00A006.

## References

[1] TESLA TDR, DESY 2001-011 (2001).

[2] GLC Project, KEK Report 2003-7 (2003).

[3] T.O. Raubenheimer *et al.*, NLC ZDR Design Group, SLAC-R-0474 (1996).

[4] Memorandum to the PRC, from the proposal 01/02, DESY, Hamburg, Memo-01, CALICE collaboration, October 2001, http://polywww.in2p3.fr/flc/calice_offic.html.

[5] A Scintillator Tile Hadron Calorimeter for the Linear Collider Detector, V. Korbel, *Proc. of 9th Topical Seminar on Innovative Particle and Radiation Detectors*, Siena (2004).

[6] Performance goals and design considerations for a linear collider calorimeter, F. Sefkow, *Proc. of Calor2004*, Perugia (2004), LC-DET-2004-022, http://www-flc.desy.de/lcnotes/.

[7] Calorimeter Design with Energy-Flow Concept, V. Morgunov *Proc. of Calor2002*, CALTECH (2002).

[8] Optimization Studies for a Scintillator-Tile to Wavelength-Shifter Fibre Light Readout for the TESLA-CALICE Tile-HCAL, V. Korbel *et al.*, to be published as LC-DET note, http://www-flc.desy.de/lcnotes/.

[9] The Scintillator Tile hadronic Calorimeter prototype R&D studies and construction plans, V. Rusinov *Proc. of 9th Topical Seminar on Innovative Particle and Radiation Detectors*, Siena (2004).

[10] G. Bondarenko, P. Buzhan, B. Dolgoshein, V. Golovin, E. Guschin, A. Ilyin, V. Kaplin, A. Karakash, R. Klanner, V. Pokachalov, E. Popova, K. Smirnov, Nucl. Instrum. Meth. A **442** (2000) 187.

[11] P. Buzhan, B. Dolgoshein, L. Filatov, A. Ilyin, V. Kantzerov, V. Kaplin, A. Karakash, , F. Kayumov, S. Klemin, A. Pleshko, E. Popova, S. Smirnov, Yu. Volkov, Proceedings of the 7th Internaional Conference on Advance Technology & Particle Physics, 717 (2002).

[12] P. Buzhan, B. Dolgoshein, L. Filatov, A. Ilyin, V. Kantzerov, V. Kaplin, A. Karakash, F. Kayumov, S. Klemin, E. Popova, S. Smirnov, Nucl. Instrum. Meth. A **504** (2003) 48 (2003).

[13] E. Garutti *et al.*, LC note, LC-DET-2004-025, http://www-flc.desy.de/lcnotes/.

[14] F. Gaede *et al.*, LC note, LC-TOOL-2003-053, http://www-flc.desy.de/lcnotes/.

[15] S. Agostinelli *et al.*, Nucl. Instrum. Meth. A **506** (2003) 250.